Earth Planets Space, **51**, 877–885, 1999

Comparison of terdiurnal tidal oscillations in mesospheric OH rotational temperature and Na lidar temperature measurements at mid-latitudes for fall/spring conditions

M. J. Taylor[1], W. R. Pendleton Jr.[1], C. S. Gardner[2], and R. J. States[2]

[1]*Space Dynamics Laboratory and Physics Department, Utah State University, Logan, Utah, U.S.A.*
[2]*Department of Electrical and Computer Engineering, University of Illinois at Urbana-Champaign, Urbana, Illinois, U.S.A.*

(Received September 3, 1998; Revised February 8, 1999; Accepted February 8, 1999)

Results from two different instrumental techniques, an Na Wind/Temperature Lidar and an OH Mesospheric Temperature Mapper, have been combined to investigate the occurrence and properties of the mid-latitude terdiurnal (8-hr) tide at near mesopause altitudes (80–105 km). High-resolution Na lidar measurements were taken throughout the diurnal and annual cycle (1996–98) at Urbana, Illinois (40°N, 88°W) to characterize the seasonal behavior of the 24, 12, 8 and 6-hr tides. Complementary measurements using a recently developed CCD imager capable of mapping OH temperature (at ∼87 km altitude) were made from Bear Lake Observatory, Utah (41.9°N, 111.6°W) and Ft. Collins, Colorado (40.6°N, 105°W) within the same time period. The "mean day" lidar data for the spring and fall periods investigated here each indicate an average amplitude variation of ∼2–5 K over the depth of the OH layer but distinct phases of <1-hr LST and ∼7-hr LST, respectively, for the 8-hr component. The Temperature Mapper data are in excellent agreement with these findings but in addition have shown that the amplitude of this tidal component can vary by as much as an order of magnitude (1.5–15 K) on a night-by-night basis resulting in an apparent 8-hr dominance of the nocturnal variation during investigated portions of the spring and fall seasons with little or no diurnal and semi-diurnal variability evident. Reports of terdiurnal tidal measurements in the mid-latitude nightglow emissions are exceptionally rare and have yet to be modeled. These innovative joint measurements pave the way for new research in this important area.

1. Introduction

Tides, driven in part by the absorption of solar energy at various levels in the atmosphere, play a major role in the dynamics of the mesosphere and lower thermosphere (MLT) region (altitude ∼80–105 km) impacting the wind, temperature and density structure. The theory of migrating solar atmospheric tides is well developed. They are global in scale and, due to the nature of the forcing, they exhibit periodicities equal to the solar day and its sub-harmonics (i.e., 24, 12, 8, 6, 4.8, 4-hr etc.) and appear to propagate westwards following the motion of the Sun (e.g., Chapman and Lindzen, 1970). Remote sensing investigations of the MLT region using ground-based radar (e.g., Avery *et al.*, 1989; Manson *et al.*, 1989; Vincent *et al.*, 1989; Franke and Thorsen, 1993; Thayaparan, 1997) and spaceborne optical sensors on the Upper Atmospheric Research Satellite (UARS) (e.g., Hays *et al.*, 1994; Burrage *et al.*, 1995; Shepherd *et al.*, 1995; McLandress *et al.*, 1996; Geller *et al.*, 1997) have provided a wealth of data on the local time and global scale effects of solar tides on the wind field. Together with recent model developments such as the Global Scale Wave Model (GSWM) (Hagan *et al.*, 1995; Hagan, 1996), these studies have revealed a complex, yet understandable, mean global variation that is determined primarily by the combined influences of the diurnal and semi-diurnal tidal components. However, the rather large short-term tidal variability is still incompletely understood (Hagan, 1996; Hecht *et al.*, 1998).

Studies of the influences of atmospheric tides on airglow emissions using long-term ground-based observations of the nightglow emissions were first conducted by Fukuyama (1976) and Petitdidier and Teitelbaum (1977). Several emission layers occur within the MLT region, such as the OH Meinel layer (peak height ∼87 km) and the $O_2(0, 1)$ Atmospheric layer (∼94 km), giving the opportunity to investigate vertical propagation characteristics of the tides. However, a major limitation of airglow studies is the duration of the nocturnal window providing at most ∼10–12-hr of data at low and mid-latitudes. Nevertheless, it has been shown that useful information on the tides can be extracted from data spanning less than a day depending on their length, sample rate and precision (Crary and Forbes, 1983). Airglow measurements are, therefore, of considerable importance as they provide a potentially useful measure of the induced intensity and temperature perturbations as a function of local solar time at any given site (e.g., Scheer and Reisin, 1990; Wiens *et al.*, 1995; Hecht *et al.*, 1998). Lidar studies of atmospheric tides in the MLT region were first conducted by Clemesha *et al.* (1982) using an extended series of Na density observations. A major advantage of these measurements is that they permit "24-hr" sounding of the atmosphere, a feature of considerable

importance for detailed diurnal and semi-diurnal tidal studies (e.g., Kwon *et al.*, 1987; Dao *et al.*, 1995). Most recently the development of a wind/temperature lidar with 24-hr capability by the University of Illinois has provided an exceptional opportunity to investigate the diurnal temperature and density perturbations induced by the tides throughout the MLT region (e.g., Yu *et al.*, 1997). In this paper we draw from the results of a 2-year tidal study using this system, recently reported by States and Gardner (1999b), to investigate the origin and properties of persistent 8-hr oscillations in OH rotational temperature newly identified by Pendleton *et al.* (1999).

Terdiurnal (8-hr) oscillations in the MLT wind field were first detected in meteor echo data (Revah, 1969). Subsequent radar studies (e.g., Teitelbaum *et al.*, 1989) have established this tidal oscillation as an almost permanent feature of the wind field at MLT heights. In contrast to these findings, airglow measurements yielding 8-hr oscillations are remarkably sparse, and only recently have their existence at high latitudes (Sivjee *et al.*, 1994; Oznovich *et al.*, 1995) and mid-latitudes (Wiens *et al.*, 1995) been reported. The isolated observations of Wiens and colleagues were based on five nights of $O_2(0, 1)$ Atmospheric band data recorded at Bear Lake Observatory (BLO), Utah during mid-April, 1993. They determined that a best-fit model for their nocturnal intensity and temperature data was dominated by an 8-hr component with no diurnal or semi-diurnal signatures detectable. As part of a more detailed investigation of the occurrence and properties of this tidal component at mid-latitudes, we have analyzed novel data obtained using the CEDAR Mesospheric Temperature Mapper (MTM) located initially at BLO and later at Ft. Collins, Colorado. This instrument images the near infrared (NIR) OH emission at spectrally isolated wavelengths and provides a precise (<1 K) measure of 30-min averaged atmospheric temperature at ~87 km altitude. Persistent 8-hr oscillations that dominated the nocturnal atmospheric temperature variability were observed on many occasions during the spring and fall periods where our analyses to date have focused. The properties of these waves have recently been reported by Pendleton *et al.* (1999). Here we compare these new airglow results with recently reported lidar measurements of the terdiurnal tide at Urbana, Illinois (States and Gardner, 1998b). Together these two autonomous data sets have been used to perform an initial investigation of the nature of the terdiurnal oscillations imaged in the MLT temperature field and to investigate the origin of their apparent dominance of the nocturnal variability during the investigated portions of the spring and fall seasons.

2. Instrumentation and Analysis Techniques

Over the past two years (1996–1998) extensive, near simultaneous temperature measurements of the upper mesospheric region have been made independently using two state-of-the-art instruments: a powerful Na Wind/Temperature Lidar system (University of Illinois) and an OH Mesospheric Temperature Mapper (Utah State University). The lidar system, located at Urbana (40°N, 88°W), has been operated for several days each month to obtain continuous 24-hr measurements of the 80–105 km region. Observations commenced in February 1996 and continued until January 1998 providing an exceptional data base for investigating the diurnal and seasonal variability of the mesopause region (States and Gardner, 1999a,b). In parallel with these measurements, nocturnal observations using a recently developed OH Mesospheric Temperature Mapper were made initially from BLO (41.9°N, 111.6°W) during the fall of 1996 and Spring of 1997 and then on a monthly basis from June 1997 to June 1998 from Ft. Collins (40.6°N, 105°W) in collaboration with C. Y. She (Colorado State University).

2.1 Mesospheric temperature mapper

The Mesospheric Temperature Mapper (MTM) is a new instrument that was developed under the US CEDAR (Coupling, Energetics and Dynamics of Atmospheric Regions) program to provide enhanced imaging capabilities for upper atmospheric research. The primary design requirement for the instrument was to map short period (10–60 min) mesospheric gravity wave signatures in the near infrared (NIR) OH Meinel nightglow emission which arises from a well-defined layer at a mean altitude of ~87 km (e.g., Baker and Stair, 1988). However, the imager has also proven to be exceptionally capable of measuring much longer period inertial-type gravity waves and tidal disturbances of periodicities up to ~12 hr (limited by the duration of the nocturnal data set). The MTM design is based on a proven photometric technique to determine mesospheric temperature using intensity ratios of selected OH M (6, 2) P_1-branch rotational lines (e.g., Meriwether, 1975). The transition probability ratio used for the rotational temperature determinations is $\{A[P_1(4)]/A[P_1(2)]\} = 1.325$ which is the average of two ratios based on the results of Mies (1974) and Langhoff *et al.* (1986). To achieve high signal-to-noise ratio images (~80–100:1) necessary for precise (~1–2 K) temperature determinations the MTM utilizes a high performance solid state (CCD) camera incorporating a large area (6.45 cm^2) back thinned array of quantum efficiency, ~80% at visible wavelengths, and ~50% at near infrared (NIR) wavelengths. The optical arrangement comprises a large format 6 × 7 cm Pentax primary lens providing a 75° field of view. A fast, f/5.6, telecentric lens arrangement is used to image the faint nightglow signals through two narrow band (~1.2 nm full-width at half maximum, FWHM) interference filters centered on the $P_1(2)$ and $P_1(4)$ OH M (6, 2) rotational lines at 840.0 nm and 846.5 nm, respectively. This signal is then re-imaged onto a 1024 × 1024 pixel CCD array whose low dark current (0.1 electrons/pixel/sec), low read noise (3.6 electrons RMS) and high linearity (0.03%) provide an exceptional capability for quantitative measurements of the faint OH ro-vibrational transitions (Taylor and Pendleton, 1996).

A computer controlled, temperature stabalized filter wheel is used to select each emission in turn. In the current application, sequential 1-min exposures of the $P_1(2)$ and $P_1(4)$ lines, followed by a background measurement at 857 nm, were used to determine rotational temperatures at the rate of about 18 samples/hour (i.e., one every 3 minutes). The well blocked three cavity interference filters provide adequate isolation of the P_1 transitions of interest from neighboring P_2 transition, and in the case of the $P_1(2)$ λ-doublet from all of the higher-N″ Q-branch emissions except for the weak Q(5) components. In practice the $P_1(2)$ signal was corrected for the weak Q(5) contamination which was estimated at ~2% at

a typical mid-latitude rotational temperature of 200 K. Further details of this procedure are given in Pendleton *et al.* (1999).

To obtain the large signal-to-noise ratios necessary for high temporal resolution temperature determinations, the image data were binned on chip down to 128 × 128 superpixels providing a zenithal footprint of 0.9 × 0.9 km at OH heights which is sufficient to resolve even the shortest expected horizontal wavelength gravity waves (∼5 km) (e.g., Taylor *et al.*, 1997). However, for this study only the central 5 × 5 superpixels of the image data have been used to investigate the long period (>1 hour) wave content. This results in a reduction of the zenithal resolution to ∼5 km (facilitating comparisons with previous OH temperature determinations using Michelson interferometers) and optimizes the removal of star-field contributions from the images used to compute the rotational temperatures. An example of the zenith temperature determinations obtained using the MTM is shown in Fig. 1. The data were recorded on the night of October 6–7, 1996 from BLO in-between two over-flights of the Ballistic Missile Defence Organization (BMDO) Mid-course Space Experiment (MSX) satellite. The x's indicate individual 3-min temperature determinations during an ∼10-hr nocturnal interval (plotted in Universal Time, UT) and illustrate the typical spread in the measurements. An analysis of the statistical fluctuations associated with the individual data points indicates a standard deviation of ∼1.2 K (Pendleton *et al.*, 1999). The absolute accuracy of the measurements, based on comparisons with Michelson interferometer and Na temperature lidar measurements (P. Espy and C. Y. She, private communication), is currently less certain at ±5 K. Evident in this figure is a well-defined, quasi-monochromatic oscillation centered on a mean value of ∼195 K. This perturbation is emphasized by the solid line which shows a least-squares fit to the data indicating a periodicity of ∼8-hrs and an amplitude of ∼7 K. An 8-hr oscillation was also evident in the OH $P_1(2)$ and $P_1(4)$ intensity data (not shown), but shifted significantly in phase confirming the wave-like nature of the perturbation. Such long-period variations have now been observed on a number of nights since the inception of our MTM measurements, particularly during the spring and fall periods, and constitute the core of this study.

2.2 Na wind-temperature lidar

A powerful Na wind/temperature lidar system capable of day and night-time operation has been used to investigate the mean thermal structure of the mid-latitude mesopause region (80–105 km) (States and Gardner, 1999a) and the seasonal behavior of the solar diurnal tide and its harmonics at 12, 8, and 6-hr (States and Gardner, 1999b). The lidar, developed by the University of Illinois, has been operational at Urbana (40°N, 88°W) for almost two years in this mode acquiring ∼1000-hr of data from February 1996 to January, 1998. Detailed descriptions of this system can be found in Bills *et al.* (1991) and Bills and Gardner (1993) while a summary of the daytime modifications together with some initial results of tidal temperature and wind perturbations is presented in Yu *et al.* (1997). To reduce background noise from the bright daytime sky, the laser beam divergence and telescope field of view were reduced to 0.5 mrad. A temperature stabilized, narrowband interference filter and a pressure tuned Fabry-Perot etalon were also employed in the daytime receiving telescope to reduce the optical bandwidth to 10 GHz (FWHM) (Yu *et al.*, 1997). The resultant temporal resolution for daytime temperature measurements was 20 min and 7.5 min for nighttime measurements. The vertical resolution was 960 m throughout the diurnal cycle of measurements. Data were obtained intermittently throughout this period (depending on weather conditions), but the goal to obtain observations during three different days per month in each of the 24 one hour bins of the diurnal cycle was achieved over 80% of the time (States and Gardner, 1999b).

In order to investigate the properties of the tidal components, a mean day "24-hr" temperature profile spanning the 80–105 km region was computed for each week of the year in the following way. The temperature data were first averaged into 1-hr bins for each observation period. The data in

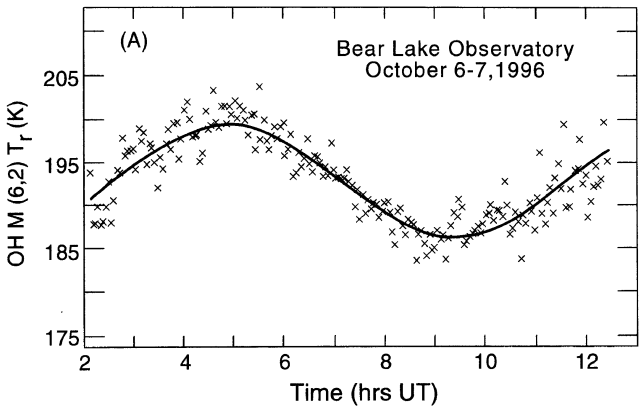

Fig. 1. Time series of OH M (6, 2) rotational temperature measurements obtained from BLO on October 6–7, 1996 illustrating a marked quasi-monochromatic oscillation (3 min/sample). The solid curve indicates the LS fit of period 8.2 ± 1.0 hr, amplitude 6.7 ± 0.9 K and phase 6.2 ± 0.8 hr LST (Pendleton *et al.*, 1999).

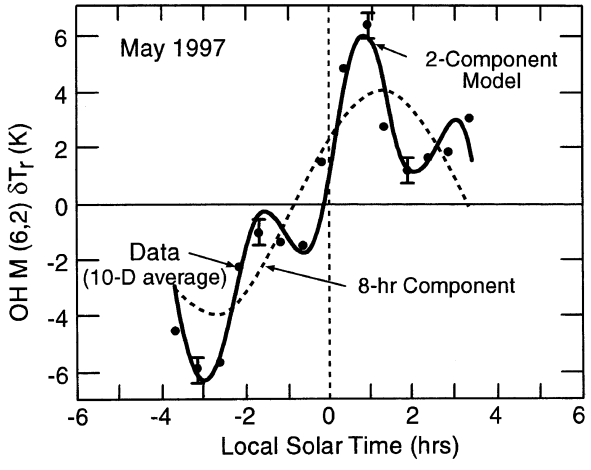

Fig. 2. Ten-day averaged OH spring nocturnal temperatures recorded at BLO for the period 4–14 May, 1997 plotted at ∼30 min intervals. The LS fit indicated by the solid curve consists of two components of periods 8-hr and ∼3-hr. The 8-hr component indicated by the dashed line has an amplitude of 4.0 ± 0.7 K and a phase of 1.2 ± 0.7 hr LST.

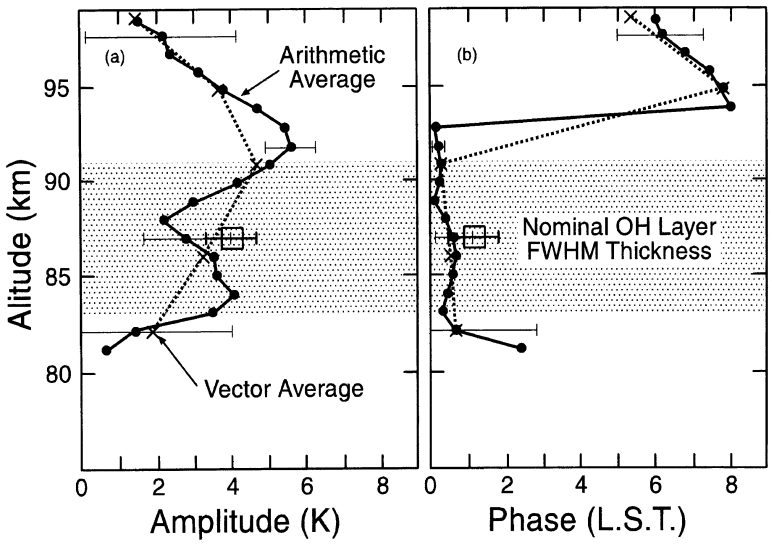

Fig. 3. Comparison of Na lidar mean spring day results for the 8-hr tide with MTM measurements of Fig. 2. Plot (a) shows the amplitude of the 8-hr tide as a function of altitude for the arithmetic average (solid line) and vector average (dashed line). Both methods indicate a mean amplitude of ~2–5 K over the nominal OH layer thickness (dotted area) which compares very favorably with the LS value of 4.0 ± 0.7 K derived from the MTM data. Plot (b) shows the corresponding phase information which exhibits little variability around the OH layer yielding a mean value of ~0.2–0.8-hr LST in good agreement with a mean MTM phase of 1.2 ± 0.7 hr.

each 1-hr bin were then weighted using a Hamming window of four weeks FWHM centered on the week of interest. The weighted data were then averaged to form a "mean day" temperature profile for each week of the year. This averaging method was chosen to eliminate any incoherent, day-to-day variability in the data, leaving only the effects of the coherent tidal oscillations (States and Gardner, 1999b). To investigate seasonal variations in the tides the diurnal data were also combined into 3-month averages each of 13 weeks period centered on the spring equinox, fall equinox, winter solstice and summer solstice.

3. Observations and Results

Both harmonic analyses, based on least-squares fitting (LS), and Fourier transform methods were used to extract information about the dominant low-frequency components evident in the MTM time series data (Pendleton *et al.*, 1999). The data of Fig. 1 show one example of the nocturnal variations recorded by the MTM. On this occasion the best fit (LS) model consisted of a single sinusoid of period 8.2 ± 1.0 hr, amplitude 6.7 ± 0.9 K and phase 6.2 ± 0.8 hr LST. Note the two sigma (95%) confidence interval is specified for the periodicity estimate to emphasize that the semi-diurnal tide and 6-hr tide are incompatible with this estimate. On other occasions more than one frequency component was observed. For example, on the night following this event (7–8 Oct.) a superposition of two sinusoids of periods 8-hr and 4-hr of almost equal amplitudes (2.7 ± 0.8 K) were required to obtain the best fit to the time series. To date, our investigations have focused on the spring and fall periods of which over 60% of the data analyzed contained a clear 8-hr wave signature demonstrating its persistent nature. This is illustrated in Fig. 2 which shows the result of averaging together ten nights of data recorded during the new moon period May 4–15, 1997 from BLO. The time series data for individual nights were first averaged into 30-min bins and then superposed to yield a mean nocturnal variation for early May (indicated by the solid circles). The range in temperature of this averaged data set was ~12 K while the precision of the individual data points was estimated at 0.5–1.0 K (indicated by the example "error bars"). The solid curve shows the result of a two component LS fit to these data points. The curve is characterized by a principal maximum at ~1-hr LST, a deep minimum at ~−3-hr LST and a secondary peak around −1.6-hr LST yielding periodicities of 8-hr and 2.7-hr for the two wave components with the 8-hr component dominant. The properties of the 8-hr wave are illustrated separately by the dashed curve which indicates a recurring oscillation of mean amplitude 4.0 ± 0.7 K and phase 1.2 ± 0.7 hr LST. Although the 2.7-hr component is statistically significant, its presence in the spring but not the fall data raises questions concerning its origin and interpretation. However, the persistent nature of the 8-hr component during the spring and fall suggests a tidal origin for these waves. As will be discussed later, Wiens *et al.* (1995) observed a similar shaped nocturnal variation in their O_2 Atmospheric nightglow measurements (peak altitude ~94 km) which were also made from BLO but somewhat earlier in the spring around mid-April, 1993. Their measurements indicated a best fit two-component combination of 8-hr and 3.4 hr. Due to the "regularity and strength" of their 8-hr component they concluded it was probably of tidal origin.

To investigate the origin of this persistent 8-hr oscillation, we now compare our MTM results with the recent Na wind/temperature lidar measurements of key tidal harmonics and their seasonal and altitudinal variability over the 80–105 MLT region (States and Gardner, 1999b). As these data encompass the OH emission layer they provide an excellent data set for this investigation. Figure 3 plots the amplitude and phase of the 8-hr tide as a function of altitude as determined

by the lidar for early May conditions (window centered on 7 May, FWHM 4 weeks). The lidar data yield an amplitude and phase measurement at each height which can be summed together to provide either an "arithmetic" or a "vector" average (e.g., Manson *et al.*, 1983). The solid line in plot (a) shows the arithmetic average of the tidal component amplitude at ~1 km resolution (with representative error bars). The amplitude of this tidal harmonic varies from ~2–5 K over the nominal OH layer thickness (~8 km FWHM) which is indicated by the shaded area. For comparison the dashed line shows the vector average of these data (plotted at ~5 km resolution) and indicates a similar range of variation over the OH layer. The open box shows the ten-day average value (4.0 ± 0.7 K) for the 8-hr component derived from the MTM data (Fig. 2). The box is plotted at a nominal (peak) altitude of 87 km and within the limits of the measurement gives exceptionally good agreement with the lidar data. Indeed, the weighted amplitude for the lidar data over the nominal OH layer thickness of 8 km centered on 87 km was 3.4 K. Plot (b) shows the corresponding phase information for the arithmetic (solid line) and vector averages (dashed line) as a function of altitude. Both indicate very little change in phase over the depth of the OH layer and a mean value in the range ~0–0.8 hr. Again this result compares very favorably with the MTM data which indicated a mean phase of 1.2 ± 0.7 hr. (Note, the MTM data are a simple arithmetic average at this stage in our analysis, but as the phase change with altitude is small, we do not expect the vector value to differ significantly from this.) Thus, both the mean amplitude and phase of the spring 8-hr wave oscillations determined from the MTM data agree well with the terdiurnal tidal components derived independently from the lidar data.

Figure 4 shows a second example of wave data obtained by the MTM during the fall period. The data were recorded from Ft. Collins on November 3–4, 1997, and as with the spring (May) data, they have been averaged into 30-min bins (with mean removed). Visual comparison of the oscillation shown in panel (a) with that of Fig. 1 (which was recorded from BLO over a year earlier) indicates considerable similarity: both exhibit a pronounced maximum around 5 UT and a corresponding minimum around 9 UT and like peak-to-peak variations of ~16 K. However, in this case the November data are best represented by a two component model (solid line) of periodicity 8-hr and 12-hr, with the 8-hr wave dominant. (Note: the increased scatter in the data points around 8-10 UT was associated with the passage of a much smaller scale, shorter period gravity wave evident in the individual MTM images.) Panel (b) shows the properties of the 8-hr component. Quantitative comparisons of this wave event with that observed on October 6–7, 1996, do indeed indicate very similar perturbations of amplitudes 7.7 ± 1.3 K (vs. 6.7 ± 0.9 K, Oct.) and phases 6.5 ± 1.1 hr (vs. 6.2 ± 1.0 hr, Oct.). Panel (c) shows the 12-hr component to the LS fit for the Nov. 3–4 data. The properties of this wave will be discussed in more detail later, but it is sufficient to note here that its amplitude and phase were such as to enhance the apparent amplitude of the nocturnal variation (as evident in panel (a)).

Although a large amount of image data were obtained from Ft. Collins during the fall 1997 and spring 1998 periods, we have yet to analyze them in sufficient detail to perform a meaningful superposed epoch analysis of the type shown in Fig. 2. Comparisons of the fall results with the Na lidar tidal measurements are therefore limited at this stage. Figure 5 shows the amplitude and phase of the 8-hr tide representative of the fall period (window centered on mid-October, FWHM 4 weeks) as a function of altitude derived from the lidar data. To aid comparison with the spring data the arithmetic and vector designations are identical to that of Fig. 3. However, in this case the lidar data are compared with just two nights of MTM data (Oct. 6–7 '96 and Nov. 3–4 '97) indicated by the solid circles at the 87 km level. On average, the fall lidar amplitudes are quite comparable with the spring levels of ~2–5 K over the height range of the OH layer and both show a minimum of about 2–3 K within the OH layer (around 86–88 km) with maximum values (up to 5 K) at the layer extremities. However, each MTM event indicates a wave amplitude that was significantly larger (by a factor of ~2) than the fall mean lidar values. This is illustrated in panel (a) which plots the MTM data points at only half their observed values of 7.7 and 6.7 K. In comparison, the observed phase of these two wave events agrees well with the fall mean lidar data (within the precision of the measurements), and indicates a relatively constant value of ~7–7.5 hr LST over the

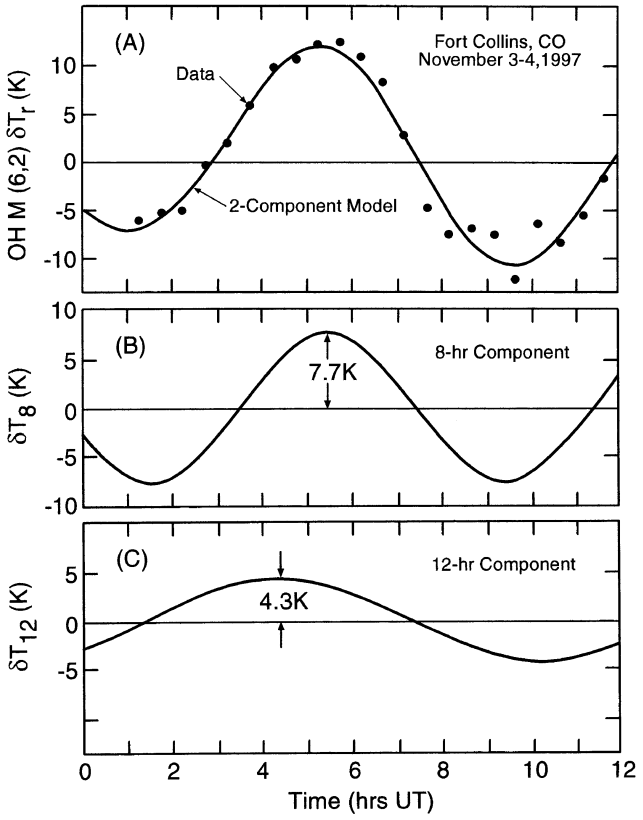

Fig. 4. (a) Example of OH temperature perturbation and LS (solid curve) model for fall data recorded at Ft. Collins on November 3–4, 1997. The data are well represented by a two-component model of periodicities 8-hr and 12-hr. (Note the increased scatter in the data points around 8–10 UT are due to passage of much smaller scale, shorter period gravity waves.) (b) Illustration of the 8-hr component (amplitude 7.7 ± 1.3 K, phase 6.5 ± 1.1 hrs). (c) Illustration of the 12-hr component (amplitude 4.3 ± 1.1 K, phase 9.6 ± 2.0 hr LST) (Pendleton *et al.*, 1999).

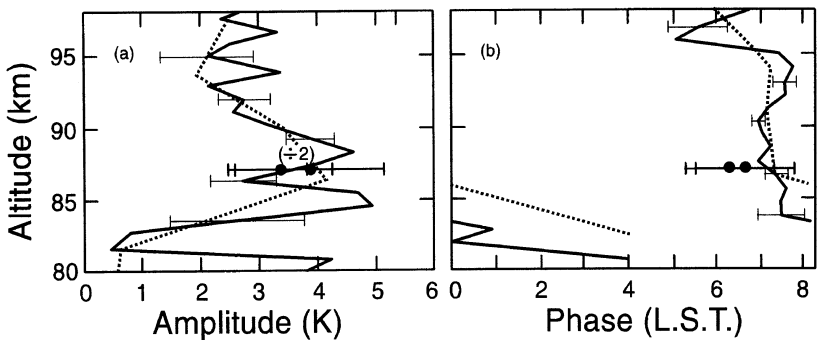

Fig. 5. Comparison of the fall mean day lidar data for the 8-hr tidal measurements with MTM measurements obtained on 6–7 October, 1996 and 3–4 November, 1997. In both cases the amplitude of the wave (indicated by solid circles) was significantly larger (~factor two) than the mean value of 2–5 K within the OH layer. The phase profile again suggests little variability throughout the OH layer with a mean value of 7–7.5-hr LST in good agreement with the individual wave phase measurements.

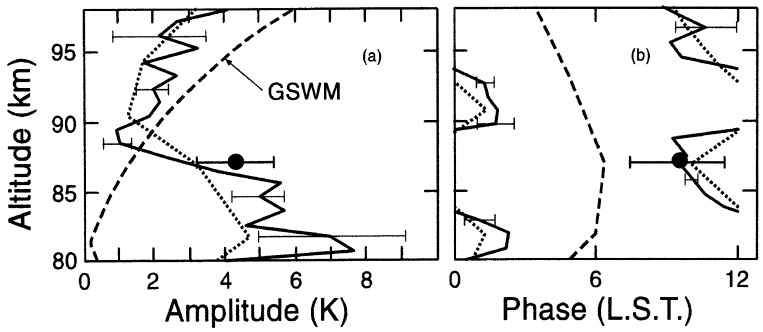

Fig. 6. Comparison of the fall mean day lidar data for the 12-hr tidal component with the MTM measurements of 3–4 November, 1997 and the GSWM predictions. The LS amplitude (4.3 K) and phase (9.6-hr LST) agree very well with the lidar data. In comparison the GSWM under predicts both the amplitude and the phase of this tidal component over the OH layer.

width of the OH layer (as compared with <1 hr LST for the spring terdiurnal tide). Thus, although the phase of the waves are in good agreement the individual fall amplitudes are significantly larger than both the arithmetic and vector means derived from the lidar data.

4. Discussion

The results of this comparative study speak for themselves: the excellent agreement in both amplitude and phase between the MTM and lidar measurements during the spring time leave little doubt that the 8-hr oscillations frequently detected in the airglow image data are of tidal origin. The same conclusion can be drawn for the fall data as the lidar measurements show that the major difference between the spring and the fall terdiurnal tide lies in a change of phase, and as Fig. 5 shows, the MTM data exhibit a significant phase shift comparable to the fall lidar value. The apparent discrepancy in amplitude between the fall lidar and MTM data can be attributed to the fact that insufficient image data were available for a comparison of average values. For example, it is well known that tidal amplitudes and phases vary significantly from day-to-day and can be much higher (or lower) than their mean values when measured over limited periods of time. The two fall "events" used in this study may, therefore, not have exhibited amplitudes representative of the mean fall value. This fact is exemplified by the spring (May) image data set which was found to contain a range of amplitudes for the 8-hr component varying from 1.5 to 7 K during the 10 days of observations but yielding an arithmetic average value of 4.0 K. Indeed, nightly amplitudes for the 8-hr temperature oscillation measured to date by the MTM indicate a range of 1.5–15 K. In each case, the phase of the 8-hr wave appears to be somewhat bi-modal, with mean values centered near 1.5 and 6 hr LST (i.e., ~180° phase shift) corresponding primarily to the spring and fall conditions respectively (Pendleton *et al.*, 1999). The striking similarity between the imager and lidar phase measurements for both the spring and fall 8-hr components, as measured in local solar time, are therefore strongly suggestive of a migrating tide. However, the separation in longitude between the lidar and imager sites (~17–23°) and the uncertainties in the phase estimates preclude a more definitive study here.

Figure 6 compares the fall mean day lidar data (~30 day average centered on autumnal equinox) for the 12-hr tide with the OH imager results of 3–4 November, 1997 (Fig. 4(c)). Both the amplitude (4.3 ± 1.1 K) and phase (9.6 ± 2.0 hr LST) of this isolated measurement (indicated by the solid circle) are in good agreement with the lidar data (amplitude

3.6 K, phase 9.7 hr LST at 87 km) further reinforcing our interpretation of these temperature perturbation data as tidal in origin. Also plotted on this figure are the model predictions for amplitude and phase using the Global Scale Wave Model (GSWM) (Hagan *et al.*, 1995; Hagan, 1996) which is based on the linear tidal model of Forbes (1982) and includes recent updates on diurnal heating rates and tidal interactions with breaking gravity waves. The GSWM can generate seasonal averages and the predictions plotted here (long dashed line) correspond to the fall period which includes the lidar and imager results. In each case the GSWM appears to under-predict the amplitude and phase as estimated independently by the lidar and imager data. A tentative comparison with the image data alone would suggest that over the altitude range of the OH emission the GSWM under-predicts the semi-diurnal amplitude by a factor ∼2 and the phase by ∼90°. However, we would not expect precise agreement with GSWM due to the variability of the tides (amplitude and phase) through the equinox period.

To date, almost all of the information pertaining to the 8-hr tide in the MLT region comes from radar measurements (e.g., Teitelbaum *et al.*, 1989; Thayaparan, 1997) which have shown that the terdiurnal tide is almost an ubiquitous feature of the mid-latitude wind field. Unfortunately the GSWM does not routinely include a capability for estimating the 8-hr solar migrating tide. Other models such as the thermosphere-ionosphere-mesosphere-electrodynamics general circulation model (TIME-GCM) (Roble and Ridley, 1994) also do not provide information on the 8-hr tidal component. Thus, at this stage it is difficult to investigate the sources of these oscillations. However, the observations of Wiens *et al.* (1995) shed further light on their properties. Using O_2 nightglow image data recorded from BLO in conjunction with the Upper Atmospheric Research Satellite (UARS), they determined a strong 8-hr wave component in their spring data which they attributed to the terdiurnal tide. Their analysis was based on five nights of measurements of the O_2 (0, 1) band (which originates at ∼94 km) during mid-April, 1993 and also showed a stastically significant 3.4-hr oscillation, but, no evidence of diurnal or semi-diurnal signatures (see their figure 3). The clear similarity in wave content between their spring observations and our 10 day averaged May data set (Fig. 2), which was recorded from the same site but four years later, is striking. One major difference though is an apparent 180° phase shift of the 8-hr component between the OH and O_2 data. This may be due either to the short vertical wavelength of the 8-hr wave (which is expected to be ∼13 km in the summer months (States and Gardner, 1999b)) or to a change in the phase of the 8-hr component during the transition from spring to summer time conditions. Recent radar observations from London, Canada (43°N) also show evidence for a phase difference of ∼180° between 87 and 94 km for the 8-hr tide for April-May conditions (Thayaparan, 1997). Thus, the 8-hr wave component appears to be a common (dominant) features of the mid-latitude, springtime mesopause region.

The apparent influence of the 8-hr tide in the nocturnal airglow variability, particularly during the spring and fall, is intriguing given the expected dominant role of the diurnal and/or the semi-diurnal tides. (As already mentioned current tidal models do not usually include the 8-hr wave component in their code.) Figure 7 utilizes the Na lidar and MTM data to investigate this point. The solid line plots the fall mean day diurnal temperature perturbation as determined by the Na lidar for a nominal OH emission altitude of 87 km. This perturbation contains the sum of all tidal wave components and shows considerable variability (∼14 K) during the 24-hr period. Of particular interest here is the nocturnal variation (between the dashed vertical lines) which indicates a strong quasi-sinusoidal variation in temperature of period ∼8-hr that peaks shortly before local midnight and has minima after dusk and prior to dawn. For comparison the OH data for November 3–4 (Fig. 4(a)) are re-plotted here (solid circles) to demonstrate the remarkable similarity in the nocturnal variation of the two data sets (see figure caption for details). The origin of this variation is investigated in Fig. 8 which plots separately the total temperature perturba-

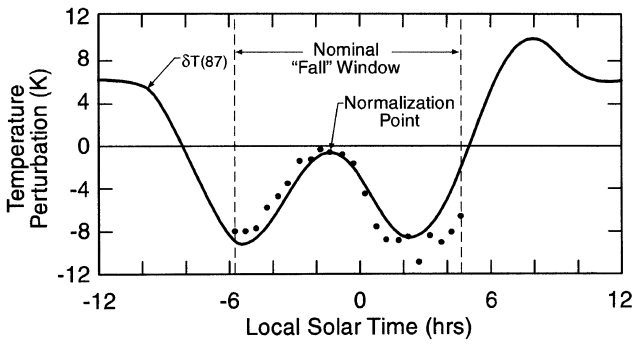

Fig. 7. Plot illustrating the diurnal variability of the fall mean day for the nominal OH altitude of 87 km. For comparison the MTM data of 3–4 November (Fig. 4(a)) are plotted (solid dots) to illustrate the remarkable similarity in nocturnal temporal behavior of the two data sets. The fit was achieved by normalizing the OH data to the peak nocturnal value of the lidar data phase shifting by −0.5-hr, and reducing the amplitude of the OH variation by a factor 0.425.

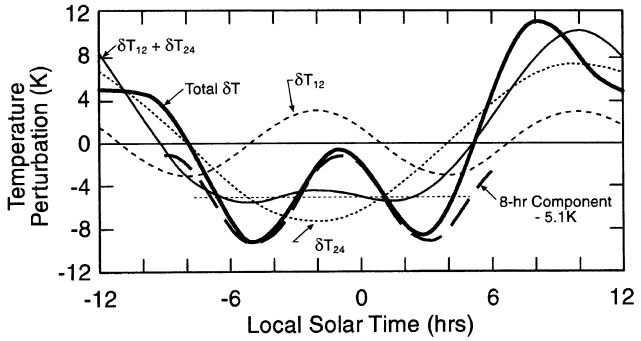

Fig. 8. Plots showing the component 24 and 12-hr tides (short dashed curves) and the total diurnal variability (thick solid curve) for the fall mean day at 87 km altitude. The sum effects of the diurnal and semi-diurnal components (thin solid curve) results in an almost flat response during the nighttime leaving the 8-hr tide to dominate the temporal variability (superposed on a DC offset of about −5 K). The dominance of the terdiurnal tide on the nocturnal variability during the fall (and spring) at mesospheric heights is illustrated in Fig. 7 and emphasized here by the long dashed curve which plots only the 8-hr component of the 3–4 November data set (see Fig. 4(b)).

tion and the 24 and 12-hr tidal components comprising the fall mean day as derived from the lidar data for 87 km altitude (States and Gardner, 1999b). The total variation (as shown in Fig. 7) is described by the thick solid line while the two short dashed curves show the 24-hr and 12-hr tidal variations. On their own each of these wave components exerts considerable nocturnal variability. However, when summed together (thin solid line) the diurnal and semi-diurnal components act to neutralize each other resulting in an almost flat nighttime response leaving the 8-hr tidal component to dominate the nocturnal variability. This is illustrated by the long dashed curve which shows the best-fit 8-hr component determined from the Nov. 3–4 data (Fig. 4(b)) superimposed on the resultant diurnal/semi-diurnal "DC offset" of −5.1 K. The close agreement between this curve and the total tidal variability (thick solid curve) confirm the dominance of the 8-hr tide on the nocturnal variability during the fall. A similar argument based on the mean spring day lidar measurements of Yu *et al.* (1997) (which form a subset of the Urbana measurements) has recently been advanced by Pendleton *et al.* (1999) to explain the dominance of the 8-hr wave in the spring nocturnal OH MTM data discussed here and the $O_2(0, 1)$ band measurements of Wiens *et al.* (1995).

5. Summary

This study combines together state-of-the-art lidar measurements of key tidal components at near mesopause altitudes with novel image measurement of OH rotational temperature using a recently developed MTM to investigate the nocturnal properties of the terdiurnal tide. As the lidar and MTM measurements were both made from similar latitude (40–42°N) sites and during the same period (1996–1998) they provide an excellent method of independently assessing the characteristics of the terdiurnal wave component. The MTM data clearly show a predominance for terdiurnal tidal signatures during the investigated portions of the spring and fall seasons governing the nocturnal variability with little or no evidence of the diurnal or semi-diurnal tides. Comparison with the fall and spring data and their characteristic amplitudes and phases agree well with those determined independently by the lidar (especially for the spring data set where sufficient imager data were available to permit a comparison of average values). Although the lidar data show a relatively low influence "on average" for the terdiurnal amplitude compared with the diurnal and semidiurnal components, the MTM data have revealed nightly wave amplitudes that varied by an order of magnitude (1.5–15 K) suggesting that on some occasions very large amplitude terdiurnal wave structure can exist. The apparent dominance of the terdiurnal tide in the nightglow data was found to be due to competing effects of the diurnal and semi-diurnal components permitting the 8-hr component to dominate during the nighttime for significant portions of both spring and fall conditions. Measurements of the thermal signature of the terdiurnal tide are uncommon, and the close agreement found in both amplitude and phase using these two different instrumental and analysis techniques reinforces and confirms our confidence in these independent measurement capabilities. A comparative lidar and imager study of the occurrence and properties of the terdiurnal tide during other seasons will be the subject of a future report (although it is interesting to note here that Wiens *et al.* (1995) found no evidence for their existence in the O_2 data obtained at BLO during the winter 1993). It is hoped that these measurements will stimulate new theoretical and modeling investigation on the seasonal behavior of the terdiurnal tide, which clearly plays an important role in the nocturnal MLT variability at least during portions of the spring and fall seasons.

Acknowledgments. Financial support for the development and operation of the CEDAR Mesospheric Temperature Mapper was provided by the National Science Foundation (NSF), grant ATM-9612810. Two of us (MJT and WRP) also acknowledge support from the Air Force Research Laboratory through contract F19628-93-C-0165. The wind/temperature lidar measurements and analyses were supported by NSF grant ATM 94-03036 and by NASA UARS grant NAG 5-2746. We are most grateful to C. Y. She (Colorado State University) for valuable logistical support during the MTM measurements at Ft. Collins. In particular we acknowledge, L. C. Gardner, V. Vasoli, M. White, J. Yu and X. Chu for their help in collecting these joint data sets.

References

Avery, S. K., R. A. Vincent, A. Phillips, A. H. Manson, and G. J. Fraser, High latitude tidal behavior in the mesosphere and lower thermosphere, *J. Atmos. Terr. Phys.*, **51**, 595–508, 1989.

Baker, D. J. and A. T. Stair, Jr., Rocket measurements of the altitude distributions of the hydroxyl airglow, *Phys. Scr.*, **37**, 611–622, 1988.

Bills, R. E. and C. S. Gardner, Lidar observations of the mesopause region temperature structure at Urbana, *J. Geophys. Res.*, **98**, 1011–1021, 1993.

Bills, R. E., C. S. Gardner, and C. Y. She, Narrowband lidar technique for sodium temperature and Doppler wind observations of the upper atmosphere, *Opt. Eng.*, **30**, 13–21, 1991.

Burrage, M. D., M. E. Hagan, W. R. Skinner, D. L. Wu, and P. B. Hays, Long-term variability in the solar diurnal tide observed by HRDI and simulated by the GSWM, *Geophys. Res. Lett.*, **22**, 2641–2644, 1995.

Clemesha, B. R., D. M. Simonich, P. P. Batista, and V. W. J. H. Kirchhoff, The diurnal variation of atmospheric sodium, *J. Geophys. Res.*, **87**, 181–186, 1982.

Crary, D. J. and J. M. Forbes, On the extraction of tidal information from measurements covering a fraction of a day, *Geophys. Res. Lett.*, **10**, 580–582, 1983.

Chapman, S. and R. S. Lindzen, *Atmospheric Tides*, pp. 125–151, D. Reidel, Dordrecht, Holland, 1970.

Dao, P. D., R. Farley, X. Tao, and C. S. Gardner, Lidar observations of the temperature profile between 25 and 103 km: Evidence of strong tidal perturbations, *Geophys. Res. Lett.*, **22**, 2825–2828, 1995.

Forbes, J. M., Atmospheric tides,1, Model description and results for the solar diurnal component, *J. Geophys. Res.*, **87**, 5222–5240, 1982.

Franke, S. J. and D. Thorsen, Mean winds and tides in the upper middle atmosphere at Urbana (40°N, 88°W) during 1991–1992, *J. Geophys. Res.*, **98**, 18,607-18,615, 1993.

Fukuyama, K., Airglow variations and dynamics in the lower thermosphere and upper mesosphere-1. Diurnal variation and its seasonal dependency, *J. Atmos. Terr. Phys.*, **38**, 1279–1287, 1976.

Geller, M. A., B. V. Khattatov, V. A. Yudin, and M. E. Hagan, Modeling the diurnal tide with dissipation derived from UARS/HRDI measurements, *Ann. Geophys.*, **15**, 1198–1204, 1997.

Hagan, M. E., Comparative effects of migrating solar sources on tidal signatures in the middle and upper atmosphere, *J. Geophys. Res.*, **101**, 21,213–21,222, 1996.

Hagan, M. E., J. M. Forbes, and F. Vial, On modeling migrating solar tides, *Geophys. Res. Lett.*, **22**, 893–896, 1995.

Hays, P. B., D. L. Wu, M. D. Burrage, D. A. Grell, H. J. Grassl, R. S. Lieberman, A. R. Marshall, Y. T. Morton, D. A. Ortland, and W. R. Skinner, Observations of the diurnal tide from space, *J. Atmos. Sci.*, **51**, 3077–3093, 1994.

Hecht, J. H., R. L. Walterscheid, R. G. Roble, R. S. Lieberman, E. R. Talaat, S. K. Ramsay Howat, R. P. Lowe, D. N. Turnbull, C. S. Gardner, R. States, and P. D. Dao, A comparison of atmospheric tides inferred from observations of the mesopause during ALOHA-93, with the model predictions of the TIME-GCM, *J. Geophys. Res.*, **103**, 6307–6321, 1998.

Kwon, K. H., C. S. Gardner, D. C. Senft, F. L. Roesler, and J. Harlander, Daytime lidar measurements of tidal winds in the mesospheric sodium layer, *J. Geophys. Res.*, **92**, 8781–8786, 1987.

Langhoff, S. R., H.-J. Werner, and P. Rosmus, Theoretical transition probabilities for the OH Meinel system, *J. Molec. Spectrosc.*, **118**, 507–529, 1986.

Manson, A. H., C. E. Meek, and J. B. Gregory, The semi-diurnal tide at the equinoxes: MF radar observations for 1978–1982 at Saskatoon (52°N, 107°W), *J. Atmos. Sci.*, **40**, 969–976, 1983.

Manson, A. H., C. E. Meek, H. Teitelbaum, F. Vial, R. Schminder, D. Kurschner, M. J. Smith, G. J. Fraser, and R. R. Clark, Climatologies of semi-diurnal and diurnal tides in the middle atmosphere (70–110 km) at middle latitudes (40–55°), *J. Atmos. Terr. Phys.*, **51**, 579–593, 1989.

McLandress, C., G. G. Shepherd, and B. Solheim, Satellite observations of thermospheric tides: Results from the wind imaging interferometer on UARS, *J. Geophys. Res.*, **101**, 4093–4114, 1996.

Meriwether, J. W., High latitude airglow observations of correlated short-term fluctuations in the hydroxyl Meinel 8–3 band intensity and rotational temperature, *Planet. Space Sci.*, **23**, 1211–1221, 1975.

Mies, F. H., Calculated vibrational transition probabilities of OH ($X^2\Pi$), *J. Molec. Spectrosc.*, **53**, 150–188, 1974.

Oznovich, I., D. J. McEwen, and G. G. Sivjee, Temperature and airglow brightness oscillations in the polar mesosphere and lower thermosphere, *Planet. Space Sci.*, **43**, 1121–1130, 1995.

Petitdidier, M. and H. Teitelbaum, Lower thermosphere emissions and tides, *Planet. Space Sci.*, **25**, 711–721, 1977.

Pendleton, W. R., Jr., M. J. Taylor, and L. C. Gardner, Terdiurnal oscillations in OH Meinel rotational temperatures for near equinoctial conditions at Bear Lake Observatory (41.9°N), *J. Geophys. Res.*, July, 1999 (submitted).

Revah, I., Etude des vents de petite echelle observes au moyen des trainees metoriques, *Ann. Geophys.*, **25**, 1–45, 1969.

Roble, R. G. and E. C. Ridley, A thermospheric-ionospheric-mesospheric-electrodynamics general circulation model (TIME-GCM): Equinox solar cycle minimum simulations (50–500 km), *Geophys. Res. Lett.*, **21**, 417–420, 1994.

Scheer, J. and E. R. Reisin, Rotational temperatures for OH and O_2 airglow bands measured simultaneously from El Leoncito (31°48′S), *J. Atmos. Terr. Phys.*, **52**, 47–45, 1990.

Shepherd, G. G., C. McLandress, and B. H. Solheim, Tidal influence on O(^{1}S) airglow altitudes and emission rates at the geographic equator observed by WINDII, *Geophys. Res. Lett.*, **22**, 275–278, 1995.

Sivjee, G. G., R. L. Walterscheid, and D. J. McEwen, Planetary wave disturbances in the Arctic winter mesopause over Eureka (80°N), *Planet. Space Sci.*, **42**, 973–986, 1994.

States, R. J. and C. S. Gardner, Temperature structure of the mesopause region (80–105 km) at 40°N latitude: 1. Seasonal variations, *J. Atmos. Sci.*, 1999a (in press).

States, R. J. and C. S. Gardner, Temperature structure of the mesopause region (80–105 km) at 40°N latitude: 2. Diurnal variations, *J. Atmos. Sci.*, 1999b (in press).

Taylor, M. J. and W. R. Pendleton, Jr., CEDAR mesospheric temperature mapper for investigating short period gravity waves, *The CEDAR Post*, **29**, 31–2, 1996.

Taylor, M. J., W. R. Pendleton, Jr., S. Clark, H. Takahashi, D. Gobbi, and R. A. Goldberg, Image measurements of short-period gravity waves at equatorial latitudes, *J. Geophys. Res.*, **102**, 26,283–26,299, 1997.

Teitelbaum, H., F. Vial, A. H. Manson, R. Giraldez, and M. Massebeuf, Nonlinear interaction between the diurnal and semidiurnal tides: Terdiurnal and diurnal secondary waves, *J. Atmos. Terr. Phys.*, **51**, 627–634, 1989.

Thayaparan, T., The terdiurnal tide in the mesosphere and lower thermosphere over London, Canada (43°N, 81°W), *J. Geophys. Res.*, **102**, 21,695–21,708, 1997.

Vincent, R. A., T. Tsuda, and S. Kato, Asymmetries in mesospheric tidal structure, *J. Atmos. Terr. Phys.*, **51**, 609–616, 1989.

Wiens, R. H., S. P. Zhang, R. N. Peterson, and G. G. Shepherd, Tides in emission rate and temperature from O_2 nightglow over Bear Lake Observatory, *Geophys. Res. Lett.*, **22**, 2637–2640, 1995.

Yu, J., R. States, S. J. Franke, C. S. Gardner, and M. Hagan, Observations of tidal temperature and wind perturbations in the mesopause region above Urbana, IL (40°N, 88°W, *Geophys. Res. Lett.*, **24**, 1207–1210, 1997.

M. J. Taylor (e-mail: mtaylor@cc.usu.edu), W. R. Pendleton Jr., C. S. Gardner (e-mail: cgardner@uiuc.edu), and R. J. States